SUPPORTING INFORMATION

Peeling Single Stranded DNA from Graphite Surface to Determine Oligonucleotide Binding Energy by Force Spectroscopy

Suresh Manohar,[a] Amber Mantz,[b] Kevin Bancroft,[b] Chung-Yuen Hui[c], Anand Jagota,[a]* and Dmitri Vezenov[b]*

Department of Chemical Engineering[a] and Department of Chemistry,[b] Lehigh University, Bethlehem, PA, 18015

and

Department of Theoretical and Applied Mechanics[c], Cornell University, Ithaca, NY, 14853.

dvezenov@lehigh.edu; anj6@lehigh.edu

1. EXPERIMENTAL METHODS

1.1. Materials. Highly ordered pyrolytic graphite was purchased from Structure Probe, Inc. Gold coated AFM tips were obtained from Budget Sensors, Inc. Disulfide-protected thiol modified polythymine, poly(dT), (5'-T_{50}-3'-O-$(CH_2)_3$-S-S-$(CH_2)_2$-OH) and polycytosine, poly(dC), (5'-C_{50}-3'-O-$(CH_2)_3$-S-S-$(CH_2)_2$-OH) were purchased from Integrated DNA Technologies, Inc. and resuspended in deionized water upon receipt. Tris(2-carboxyethyl)phosphine hydrochloride (TCEP) was purchased from TCI America. Mercaptohexanoic acid (90% purity) and aminopropyltriethoxysilane (99.8 % purity) were obtained from Sigma Aldrich and used as received. All solvents used were of ACS grade**.**

1.2. Functionalization of AFM tips. All AFM tips were cleaned either by exposure to UV-ozone for 30 minutes (T10x10/OES UV-ozone cleaner from UVOCS, Montgomeryville, PA) or oxygen plasma (using room air as source) for 1 minute on high power (PDC-001 plasma cleaner from Harrick Plasma, Ithaca, NY).[1] After UV-ozone cleaning, gold coated tips were immediately immersed in anhydrous ethanol to reduce any Au-oxides formed during cleaning.[1]

Thiol-modified ssDNA molecules were grafted onto a gold-coated AFM tip[2-5] followed by treatment with MHA, chosen to serve as the spacer molecule lowering the density of the DNA molecules[2, 3] and to provide background electrostatic repulsion

between the tip and graphite, hence reducing the non-specific tip-substrate attraction. 0.1 nM solutions of thiol modified poly(dT) or poly(dC) were prepared in 10 mM phosphate buffer or 10 mM phosphate buffer saline (PBS) buffer with 1 M ionic strength (NaCl). The thiol groups were deprotected by adding 15 mg of TCEP to 10 mL of solution at least 30 min before deposition of the HS-DNA. Tips were submerged in the solution of thiol modified DNA for 1 h, rinsed with ethanol, and dried in a stream of nitrogen. The tips were then placed in 3 mM ethanolic solutions of MHA for 1 h, rinsed with ethanol, and nitrogen dried.

Deposition of DNA from low salt buffers reduces surface coverage[2] and independent XPS studies of the composition of thiolate DNA/MHA monolayers were carried out on Au coated planar Si wafers. Six samples were prepared for which the time spent in 0.1 nM HS-poly(dT) ranged from 0 to 120 minutes. Detailed XPS results can be found below. Samples exposed to DNA solutions for times longer than 60 min displayed expected presence of N and P in the ratio of 1.1-1.2 to 1 (2:1 is the ratio expected from the composition of the DNA oligomer, the lower value found experimentally is probably due to orientation of bases close to the substrate and/or inaccuracies in the sensitivity factors used).

1.3. Preparation of 3-aminopropyltriethoxysilane modified Si surfaces.[6, 7] The following steps were performed immediately after wet cleaning: (i) silanization in a 2% solution of APTES in anhydrous toluene for 1 hour and (ii) curing at 120°C for 1 hour. The APTES surfaces had an advancing water contact angle of 47±3°. Ellipsometry (Auto EL II ellipsometer, Rudolph Instruments) gave 4.2±0.6 Å for the thickness of the silane monolayer.

1.4. Force Spectroscopy Experiments. Force spectroscopy measurements were performed using an MFP-3D atomic force microscope (Asylum Research, Santa Barbara, CA). The graphite surface was freshly cleaved with Scotch® tape prior to each experiment and immediately placed in a fluid cell, which was then filled with approximately 2 mL of 10 mM phosphate buffer containing additional amount of NaCl in a range of concentrations from 0 mM to 1 M. The spring constant of each AFM cantilever was calibrated in buffer by the thermal fluctuations method.[8] For force spectroscopy experiments, the tip was brought into contact with graphite and pulled away, while the deflection of the cantilever and its displacement were measured at

varying tip velocities and at different locations on the graphite surface. A random sample of the Au coated tips was imaged after force measurements using Scanning Electron Microscopy to ensure that the Au coating remained intact during experiments (Figure S1). Analysis of the force-distance curves was performed using custom code written in Matlab (Mathworks, Natick, MA) or IGOR Pro (Wavemetrics, Eugene, OR).

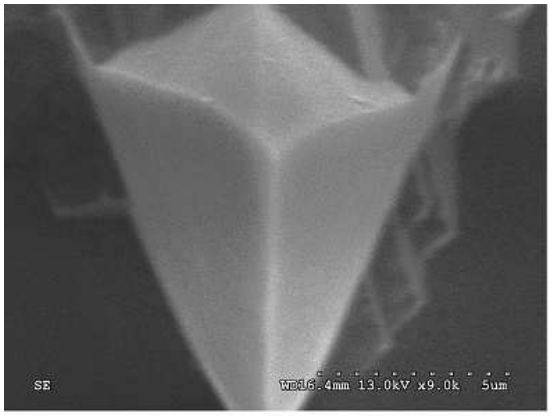

Figure S1. SEM image of gold-modified tips after FS experiments.

1.5. Fitting Single Molecule Stretching Curves to Freely Jointed Chain Model. There are two limiting cases in fitting single molecule stretching data to an extended freely jointed chain (eFJC) model. Since only one end of the DNA is anchored covalently (at the tip), the fitted contour length could represent either (i) the full length of the molecule (27 nm), if only the last few bases are sticking to the APTES surface, or (ii) part of the full length, if the part of the DNA adsorbed on the substrate breaks its contact with surface all-at-once (e.g. at a distance of 12 nm in Figure 3). To be consistent with the observed separation at pull-off, in the first case we have to assume that the DNA molecule is offset from the apex of the tip. Therefore, measured tip-surface separation does not represent true molecular extension and one needs to introduce an additional fit parameter representing the vertical offset of the attachment point of the oligonucleotide.

Starting with parameters representing either of the two limiting cases, the fits converge to two indistinguishable lines (blue line in Figure 3) of similar fit quality with the contour length of 27.5±0.18 nm in the first case and an offset of 0.00±0.80 nm in the second case. The Kuhn length and elasticity obtained for the two models were

b=1.00±0.26 nm and κ=6.2±1.5 nN, and b=0.51±0.12 nm and κ=2.4±0.8 nN. An equally good fit could be achieved for any intermediate model (short counter length and off-center molecule placement), with values of b and κ between those given above. Clearly, parameters in our eFJC model are correlated and we can only specify a range for b and κ on the basis of our force spectroscopy data.

2. INTERACTION FORCES BETWEEN GRAPHITE AND CARBOXYL TERMINATED SURFACES

We designed our force spectroscopy experiments for controlled (synthetic) DNA sequences. Since synthetic oligomers are relatively short (commercially available modified DNA is typically under 50 nm long), potential attractive interactions between the surfaces of the AFM tip and graphite can mask events related to DNA-graphite interactions and need to be mitigated. In addition, in order to observe interactions of discrete numbers of DNA oligomers, one needs to control the surface density of DNA. On gold, the density of covalent attachment of thiol-modified DNA can be readily controlled by the use of mixed self-assembled monolayers. We used a carboxyl terminated SAM that presents a charged surface at neutral pH. Using integrated intensity for S 2p and N 1s XPS peaks and assuming a well-formed thiol SAM (i.e. 0.21 nm^2 per thiol molecule), we estimated that the nearest neighbor distance between DNA strands is ~8 nm. For tips with radii of 20-30 nm, 10 to 20 DNA strands would be available for interaction with graphite when the tip contacts the surface.

Figure S2 shows a typical plot of the force versus tip-surface separation for an AFM tip functionalized with a monolayer of HS-$(CH_2)_6$-COOH in 10 mM phosphate buffer (pH 7.2). The interaction between the COOH groups on the tip and the graphite surface is repulsive everywhere. The repulsion is due to the electrical double layer formed at the negatively charged MHA interface on the AFM tip. A semi-logarithmic plot of force in the separation range of 3 nm to 10 nm from graphite (Figure S2, inset) displays a linear dependence with a decay length of 2.5 nm (extracted by fitting an exponential function to the force—separation data). The mean and standard deviation of the decay length obtained from 50 such force curves are 2.3 nm and 0.4 nm, respectively. We calculated a theoretical Debye screening length[9] of 2.1 nm for a 10 mM phosphate buffer solution. Tips modified with amino groups (APTES) also displayed

reduced non-specific interaction due to double layer repulsion with decay length of 2.7±0.2 nm (mean ± deviation) evaluated in a manner similar to analysis of MHA modified tips. The observation of repulsion for both negatively and positively charged tips suggests that the graphite surface is substantially uncharged; however, repulsion is still expected due to the confinement of ions in the small gap between the AFM tip and the surface. (See Section 5 for a derivation of repulsive forces between the AFM tip and surface.)

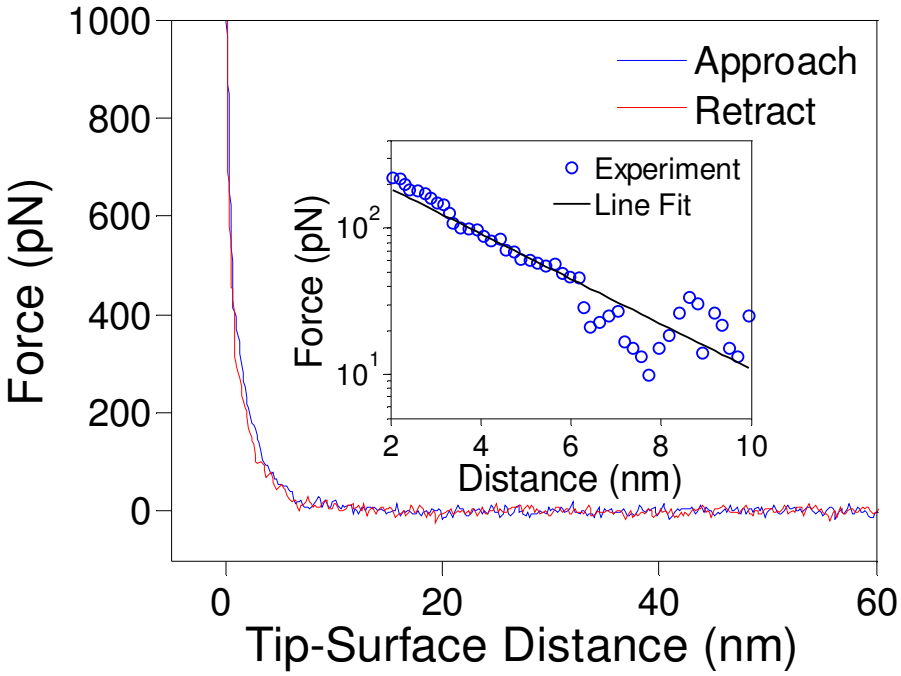

Figure S2. Typical force curve for Au-coated tip modified with HS-$(CH_2)_5$-COOH showing no adhesion between the AFM tip and the graphite substrate (tip velocity is 400 nm/s). Inset is a semi-logarithmic plot of force as a function of the separation from the surface. A linear fit yields a characteristic decay length of λ=2.5 nm, suggesting repulsion is electrostatic in nature.

3. TIPS WITH ssDNA PHYSISORBED TO AN AMINE-TERMINATED MONOLAYER.

The presence of force plateaus during tip retraction appears to be independent of how the DNA is attached to the tip surface. We observed identical features in force extension curves for covalent and non-covalent attachment. Amino-terminated silicon nitride tips showed repulsion on approach as in case of carboxyl terminated gold-coated

tips, which we again attribute to the confinement of the electrical double layer formed due to the charge of the tip surface. In contrast to MHA-modified probes, however, there was a small adhesion force (2-3 nN) on retraction. For APTES modified tips bearing physisorbed poly(dT), the interaction on approach was also first repulsive. A mean value of 2.7±0.5 nm (50 FCs) was obtained for the decay length for these tips with or without the DNA. On retraction, after the initial adhesion due to non-specific interactions between the tip and graphite, we observed steady state peeling regions (Figure S3) similar to those seen for tips functionalized with mixed thiol monolayers of poly(dT) and MHA on Au. The scatter in the average peeling force with non-covalently attached ssDNA was somewhat larger than in the case of thiol-modified ssDNA covalently bound to the tip. From characteristic steps in the force-distance curves, we obtained average values (±standard deviation) of 77±22 pN and 89±28 pN for peeling forces in two different experiments with DNA-APTES tips.

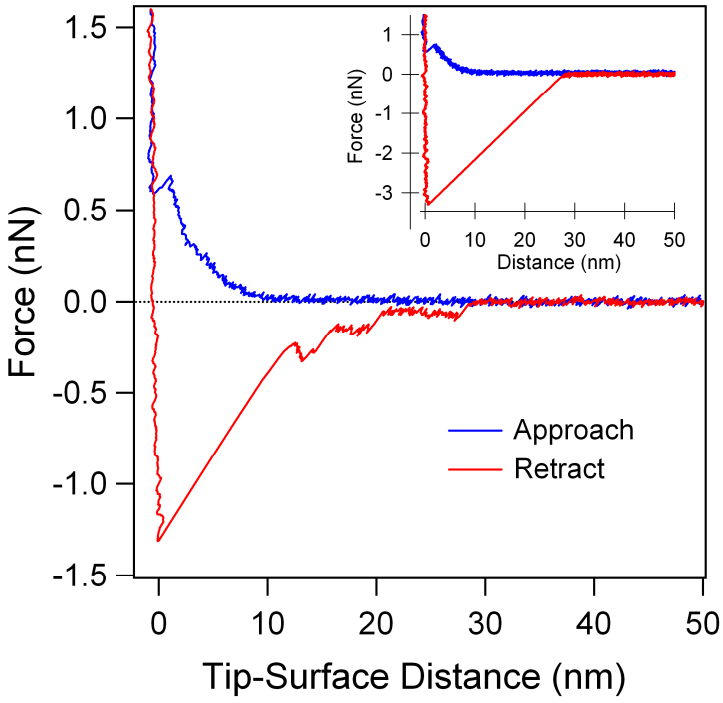

Figure S3. An example of the force-distance curve obtained in 10 mM phosphate buffer using tips terminating in amino groups and having adsorbed poly(dT). Multiple force plateaus are observed corresponding to peeling of multiple DNA strands at a steady force. Insert shows interaction between APTES modified silicon nitride tip and graphite.

4. EFFECT OF VELOCITY AND SALT CONCENTRATION ON FORCE JUMPS

Table S1. Dependence of the steady state jump force (σ is the standard deviation) on the tip velocity for the interaction between a gold-coated tip, modified with mixed monolayers of ssDNA and MHA, and graphite. The force curve data were obtained in 10 mM phosphate buffer solution.

AFM Tip Velocity (nm/s)	Force Jump ± 1 σ (pN) Poly(dT)	Force Jump ± 1 σ (pN) Poly(dC)
100		73.3 ± 6.9
200	84.2 ± 8.4	67.2 ± 3.7
400	82.3 ± 7.1	
600	79.0 ± 8.4	
1000	90.2 ± 8.8	66.2 ± 6.3

Table S2. Steady state peeling force observed between graphite and a gold coated tip modified with mixed monolayers of ssDNA and MHA in a 10 mM phosphate buffer solution with varying concentration of NaCl. Forces were recorded at a tip velocity of 200 nm/s.

NaCl Concentration (mM)	Force Jump ± 1 σ (pN) Poly(dT)	Force Jump ± 1 σ (pN) Poly(dC)
0	85.6±7.5	67.2 ± 3.7
50	82.0±5.0	
100	79.9±6.5	68.4 ± 8.6
200	81.2±4.6	
800	81.1±6.0	

14 different experiments on poly(dT) produced the following mean peeling forces: 103.90; 93.15; 93.78; 85.63, 85.57; 82.25; 79.03; 90.22; 81.98; 79.94; 81.17; 81.09; 71.80; 88.11 pN.

14 different experiments on poly(dC) produced the following mean peeling forces: 64.76; 62.08; 51.01; 73.33; 67.19; 66.19; 52.87; 56.33; 50.37; 46.65; 50.22; 68.43; 75.71; 66.49 pN.

5. XPS STUDIES OF MIXED DNA/MHA MONOLAYERS ON Au SURFACE.

Au-coated silicon wafers were functionalized with mixed monolayers of thiol modified poly(dT) as described in the experimental section. XPS experiments were performed with a Scienta ESCA300-6u spectrometer using a monochromatic Al Kα X-ray source (1486.6 eV). The BE scales for the monolayers on gold were referenced by setting the Au4f7/2 BE at 84.0 eV. All fits are performed to Voigt shape constrained to the same width and percent Gaussian for all peaks. Spectra shown in Figures S4-S6 are those from the samples prepared under the identical conditions used to prepare Au-coated AFM tips (SH-poly(dT) was deposited for 1 hour followed by 1 hour of MHA deposition).

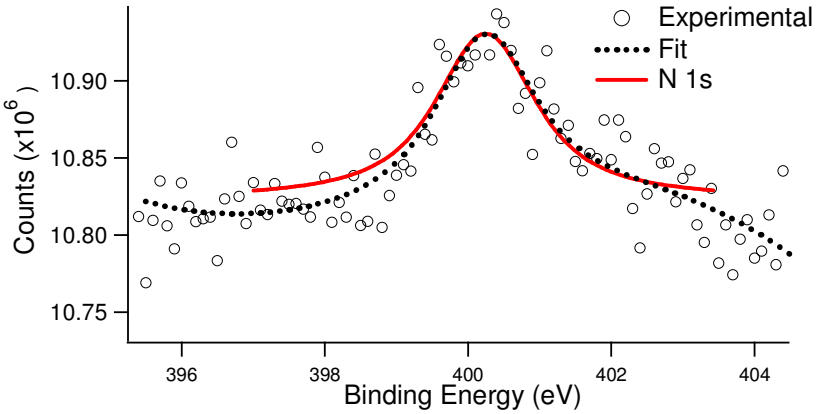

Figure S4. High resolution XPS spectrum of the N1s region.

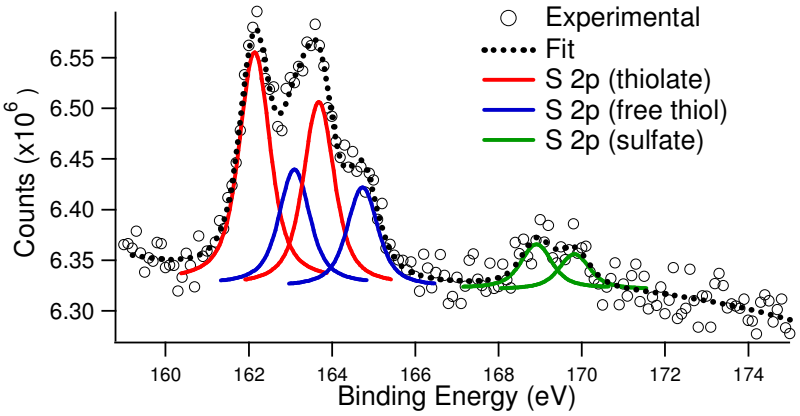

Figure S5. High resolution XPS spectrum of the S2p region.

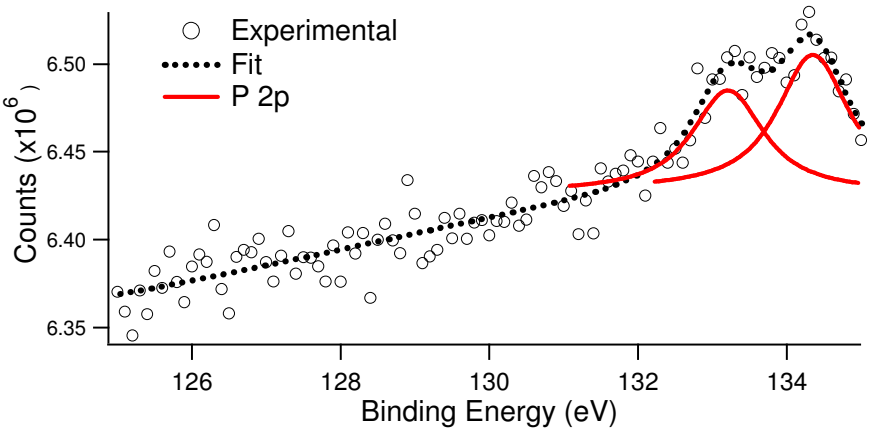

Figure S6. High resolution XPS spectrum the P2p region.

Sulfur was not apparent on either the clean gold surface or the sample prepared with DNA only. When present, the S2p spectra showed a doublet structure due to the presence of the S2p3/2 (162 eV: used in analysis above) and S2p1/2 peaks (164 eV). The BE of the S2p3/2 peak was consistent with sulfur atoms bound to the gold surface as a thiolate species. A small signal was present in the spectrum above 164 eV, here seen as a small shoulder on the S2p1/2 peak, indicating that not all sulfur species were bound to the gold surface, but that free thiol species were present (a BE of about 165 eV is expected for a free thiol species). Additionally, a small signal can be seen between 168 eV and 170 eV showing the presence of oxidized sulfur species.[5]

Nitrogen and phosphorous were only observable in the spectra obtained from samples onto which the HS-poly(dT) solution had been deposited for 60 min or 120 min. The expected ratio of N to P is 2:1. The ratio observed was about 1.1-1.2 to 1, however, the presence of these elements is good evidence of the presence of HS-ssDNA bound to the gold surface.[2, 3]

6. DEBYE LENGTH BETWEEN A CHARGED SURFACE AND A NEUTRAL SURFACE USING DEBYE HUCKEL THEORY.

Here we wish to establish the scaling of the repulsive interaction that arises between a charged AFM tip and a neutral, uncharged substrate due to confinement of ions in the space between the two. The fact that both negatively and positively charged (MHA and APTES modified) AFM tips experience a repulsive interaction with respect to

graphite suggests that the graphite surface is substantially uncharged. We represent it by the boundary condition that electric field normal to it vanishes and compute the interaction between the AFM tip and graphite using linearized Debye-Huckel (DH) theory. Because of the limited applicability of linearized DH theory, our model is not expected to be quantitatively accurate. Rather, our purpose here is only to establish that exponentially decaying repulsive forces can arise in such a situation.

Consider the case of the fixed surface charge density, σ, on the AFM tip of radius R, whereas the graphite surface is uncharged. (A similar analysis with fixed surface potential leads to a result for force with the same exponential decay in force with distance.) Using Derjaguin's approximation,[10] the force, *F*, between the AFM tip and the graphite surface can be written as

$$F = 2\pi R\, w(d) \tag{S1}$$

where *d* is the distance between the AFM tip and the graphite surface, and *w(d)* is the interaction energy per unit area between a flat plate with the same charge density and a graphite surface, separated by distance *d*.

When two parallel plates have an electrolyte solution between them, the electrostatic potential is governed by the Poisson-Boltzmann equation.[9] For small potentials, this equation can be linearized to the DH equation, which in one-dimension is,[9]

$$\frac{d^2\psi}{dx^2} = k^2\psi \tag{S2}$$

where *k* is the inverse Debye screening length. Eq. S2 has the solution of the form:

$$\psi(x) = A\cosh(kx) + B\sinh(kx) \tag{S3}$$

$$\frac{d\psi}{dx} = Ak\sinh(kx) + Bk\cosh(kx) \tag{S4}$$

Fixing the origin at the charged surface and extending the axis towards the graphite surface, we then impose the boundary conditions relating field to charge density:

$$\left.\frac{d\psi}{dx}\right|_{x=0} = \frac{\sigma}{\varepsilon\varepsilon_o} \quad \Rightarrow B = \frac{\sigma}{\varepsilon\varepsilon_o k} \tag{S5}$$

At $x=d$,

$$\left.\frac{d\psi}{dx}\right|_{x=d} = 0 \Rightarrow A = \frac{-\sigma}{\varepsilon\varepsilon_o k}\coth(kd) \qquad \text{(S6)}$$

With a little manipulation, we find

$$\psi(x) = -\frac{\sigma}{\varepsilon\varepsilon_o k}\frac{\cosh\{k(d-x)\}}{\sinh(kd)} \qquad \text{(S7)}$$

The force per unit area between can be computed as,[9, 11]

$$f = \left.\frac{\varepsilon\varepsilon_o k^2\psi^2}{2}\right|_{x=d} \qquad \text{(S8)}$$

Therefore,

$$f = \frac{\sigma^2}{2\varepsilon\varepsilon_o \sinh^2(kd)} \qquad \text{(S9)}$$

Integrating Eq. S9, we obtain

$$w(d) = \frac{\sigma^2}{2\varepsilon\varepsilon_o k}\left[\coth(kd) - 1\right] \qquad \text{(S10)}$$

Using Eq. S1, we find the force between the AFM tip and the graphite surface to be

$$F(d) = \frac{\pi R\sigma^2}{\varepsilon\varepsilon_o k}\left[\coth(kd) - 1\right] \qquad \text{(S11)}$$

For $kd >> 1$, this can be approximated as

$$F(d) = \frac{2\pi R\sigma^2}{\varepsilon\varepsilon_o k}\exp(-2kd) \qquad \text{(S12)}$$

showing that the force decays exponentially with distance. We arrive at essentially the same result (different prefactor) for the case of fixed surface potential on the AFM tip.

7. RESULTS FROM MOLECULAR DYNAMICS SIMULATIONS.

Experiments under varying salt concentration suggest that binding free energy is dominated by non-electrostatic interactions. To understand the relationship between measured binding energy and the structure, we conducted molecular dynamics simulations of the interaction between thymidine and a graphitic surface using the CHARMM program and force-field.[12, 13] The graphitic surface was modeled as three parallel graphene sheets and constrained in space for all the MD simulations. The starting structure for the MD simulation was obtained by minimizing the energy of the

base near the graphitic surface. This equilibrated thymidine molecule then was moved away from the surface in increments of 0.5 Å by applying a harmonic constraint with spring constant of 13.89 N/m to the O5' atom of the sugar ring in thymidine. After every move, the energy of base-graphite system with O5' atom constrained was minimized using Adopted-Basis Newton Raphson method for 1000 steps. The structures with minimized energy obtained after every move were placed in a 42 x 52 x 37 Å^3 water-box and used as the starting structures for the MD runs with O5' atom constrained. We followed the same MD procedure as used in the paper by Manohar *et. al.*[14] with a few modifications: (i) a time step of 2 fs was used, (ii) equilibration phase was carried out for 0.5 ns, and (iii) production phase lasted 2.6 ns. The position of the O5' atom was noted every time step during the production phase and 2.6 ns of production phase data was used to calculate the mean constraining force. The energy profile was obtained by integrating the force with respect to the distance of the O5' atom (Figure S7). In the range of O5' positions between the minimum and 0.95 nm the sugar ring comes off the surface. In the range of 0.95 to 1.1 nm, the extension is accomodated by re-orientation of the bonds around the torsional angle, χ, between the sugar ring and base. For extensions greater than 1.1 nm, the base itself is pulled-off the substrate.

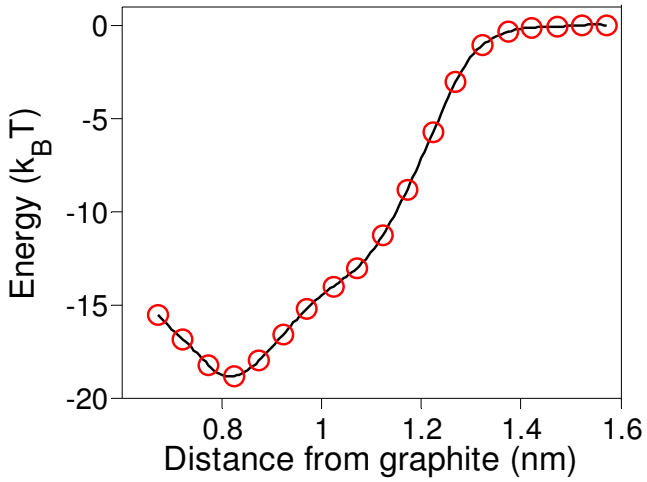

Figure S7. Binding free energy of thymidine to a graphitic surface computed by thermodynamic integration in molecular dynamics simulations using the CHARMM force field. The minimum represents an estimate of the non-electrostatic contribution to the binding free energy.

Using thermodynamic integration,[15] we computed the binding free energy between thymidine and a graphitic surface, represented by the minimum in potential energy shown in Figure S7. The energy minimum was interpreted as the binding energy of thymidine with the graphitic surface and was 18.9 k_BT, which is comparable to, but significantly larger than, the binding energy extracted from force measurements. Within the limitations of the force-field used, these simulation results support the notion that non-electrostatic contributions form the major component of the binding free energy between nucleotides and a graphene surface.

Note that the experiment measures an effective binding energy per unit length of the ssDNA backbone. For example, as suggested by Manohar *et. al.*,[14] the effective binding energy can be reduced significantly compared to that of an isolated nucleotide if some fraction of bases remain unbound due to steric hindrance from neighbors. The discrepancy could also indicate that a refinement of the force field is required for this problem.

8. EQUIVALENCE OF FORCE AND DISPLACEMENT CONTROL.

We have derived results for average number of desorbed links and average end-to-end distance of desorbed chains assuming a fixed force is applied. A natural question is whether the result depends on mode of control, in particular, if the predicted plateau force would be different under displacement control. Here we demonstrate that the predicted plateau force remains the same under force or displacement control.

Consider first the Gibbs free energy,

$$G' = U + PV - TS \tag{S13}$$

In P, T, N, R_Z ensemble:

$$dG' = -SdT + Vdp - \gamma b\, dn + f\, dR_z \tag{S14}$$

Gibbs free energy is related to the surface free energy we wish to calculate and to the force by the following two relations:

$$\left.\frac{\partial G'}{\partial R_z}\right|_{T,P,n} = f \tag{S15}$$

$$\left.\frac{\partial G'}{\partial n}\right|_{T,P,R_z} = -\gamma b \tag{S16}$$

For a FJC, we know the following:

$$\langle R_z \rangle = bn\,L\left(\frac{fb}{k_B T}\right) \tag{S17}$$

where $L(x) = \coth(x) - 1/x$ is the Langevin function. This can be inverted to obtain

$$f = \frac{k_B T}{b} L^{-1}\left(\frac{\langle R_z \rangle}{bn}\right) \tag{S18}$$

where $L^{-1}(x)$ is the inverse Langevin function. Assume that

$$\langle f \rangle = \frac{k_B T}{b} L^{-1}\left(\frac{R_z}{bn}\right) \tag{S19}$$

which is valid for large enough chains. Integrate Eq. S15 to get

$$G'(P,T,n,R_z) = \frac{k_B T}{b}\int L^{-1}\left(\frac{R_z}{bn}\right) dR_z - k_B T C(n) \tag{S20}$$

where *C(n)*, a function of *n*, is the constant of integration. Change variables to $x = R_z / bn$ to get

$$G(P,T,n,R_z) = k_B T n \int L^{-1}(x)\,dx - k_B T C(n) \tag{S21}$$

Now get the condition

$$\begin{aligned} &\left.\frac{\partial G}{\partial n}\right|_{T,P,R_z} = k_B T\left[\int L^{-1}(x)\,dx - \frac{R_z}{bn} L^{-1}\left(\frac{R_z}{bn}\right)\right] - k_B T \frac{dC}{dn} = -\gamma b; \\ &\frac{R_z}{bn} L^{-1}\left(\frac{R_z}{bn}\right) - \int L^{-1}(x)\,dx + \frac{dC}{dn} = \frac{\gamma b}{k_B T} \end{aligned} \tag{S22}$$

This equation can be solved for the unknown, R_z / bn. With the choice, $C(n) = n\ln(4\pi)$, the left hand side of Eq. S22 is

$$\begin{aligned} &\frac{R_z}{bn} L^{-1}\left(\frac{R_z}{bn}\right) - \int L^{-1}(x)\,dx + \ln(4\pi) = \frac{R_z}{bn} L^{-1}\left(\frac{R_z}{bn}\right) - \frac{R_z}{bn} L^{-1}\left(\frac{R_z}{bn}\right) + \\ &\qquad\qquad \int x\,d\left(L^{-1}(x)\right) + \ln(4\pi) \\ &= \int x\,d\left(L^{-1}(x)\right) + \ln(4\pi) \\ &= X \end{aligned} \tag{S23}$$

From Eqs. S22 and S23, we have

$$\frac{\gamma}{k_B T} = X \tag{S24}$$

Thus, Eq. S23, derived under displacement control, gives the same condition for plateau force as Eq. 5 (in main text), derived under force control.

9. REPRESENTATIVE FORCE-DISTANCE CURVES.

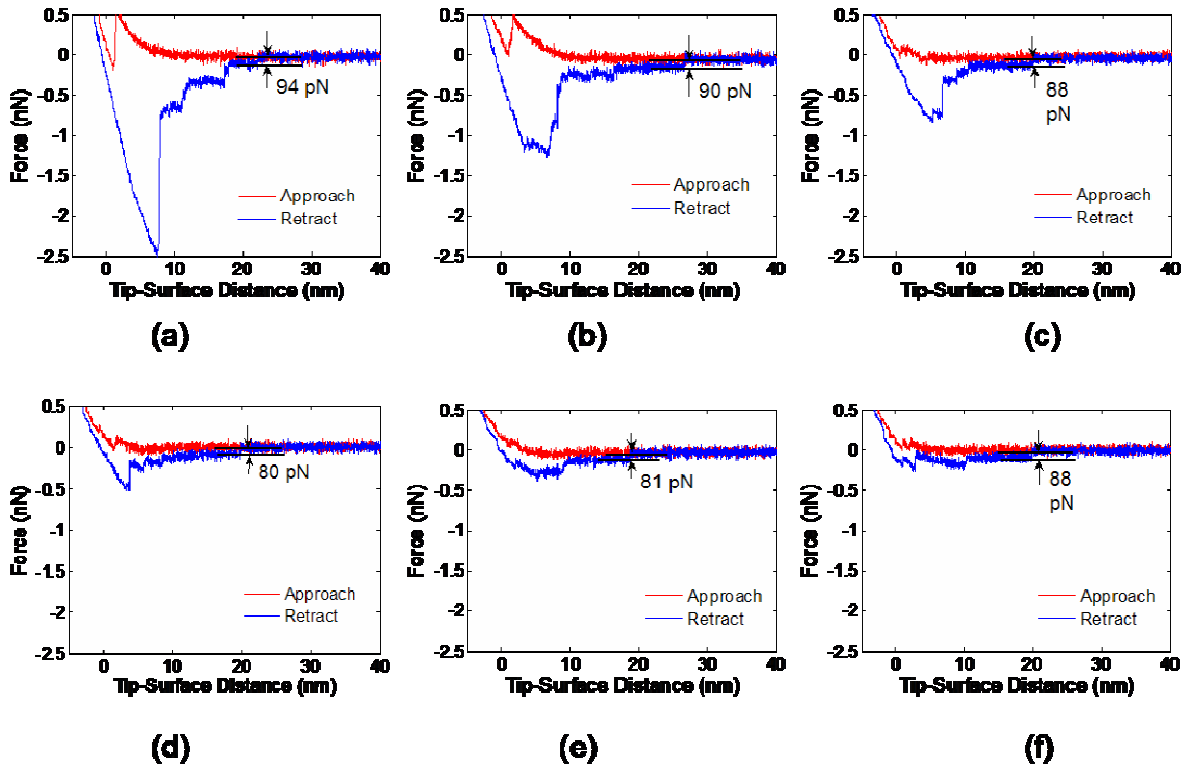

Figure S8. Six examples of force-distance curves from different experiments. Note that the initial pull-off force, which we interpret as representing multiple chain removal, varies considerably. However, force plateaus appear consistently with a force jump in a relatively narrow range. We interpret this feature of the experiment to be due to peeling of individual chains.

10. JUSTIFICATION FOR EQUILIBRIUM FOR A FIXED NUMBER OF ADSORBED BASES.

To estimate whether the experimental time scale is much larger than the equilibration time scale, we first estimate the diffusion coefficient of a segment of the polymer using the Stokes-Einstein relation:[16]

$$D = \frac{kT}{6\pi\eta b} \sim 3\,x\,10^{-10}\ \ m^2 / s \qquad \text{(S25)}$$

using viscosity of water, and *2b* ~ Kuhn length of ssDNA (*b* ~ 1nm). To estimate the diffusion coefficient of a segment on the surface of graphite, we conducted molecular dynamics simulations of a single nucleotide adsorbed on graphite and free to diffuse on the surface (Figure S9(a)). In Figure S9(b), we plot the resulting mean square end-to-end distance of the path followed by the centroid of the diffusing nucleotide as a function of distance. From the slope of these data we extract the diffusion coefficient of $7.5{\cdot}10^{-10}$ m²/s.

(a) (b)

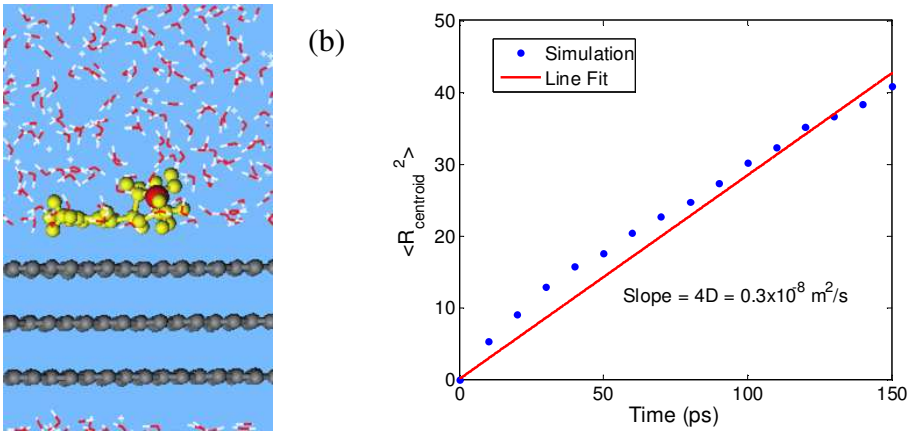

Figure S9. Estimate of diffusion coefficient of DNA nucleotide on graphite using molecular dynamics simulations (CHARMM) nucleotide at the graphite/water interface, (b) mean square distance (Å²) as a function of time.

Using the smaller of these two diffusion coefficients, we now compare the time for autodiffusion over the length of the entire molecule with the time in experiments to pull the entire length of oligonucleotide. If a Kuhn length can diffuse over distances equal to the entire length of the molecule in time much smaller than the time to pull off the entire molecule, then we can safely assume equilibrium. Typical molecular lengths in our experiment are 30 nm, and

$$4Dt_{diffusion} = \left\langle r^2 \right\rangle \qquad \text{(S26)}$$

yield an estimate of

$$t_{diffusion} = \frac{\left\langle r^2 \right\rangle}{4D} = 7.5{\cdot}10^{-7}\ \ s\,. \qquad \text{(S27)}$$

Experimental time to pull the entire molecule at the highest rate used in the experiment is

$$t_{\exp} = \frac{r}{v_{tip}} = \frac{30 \cdot 10^{-9} m}{10^{-6} m/s} = 3.0 \cdot 10^{-2} s \qquad \text{(S28)}$$

The experimental time scale is much greater than the diffusion time scale, and we may assume equilibrium under these conditions.

11. JUSTIFICATION FOR EQUILIBRIUM WITH VARIABLE NUMBER OF ADSORBED BASES.

We now present a simple kinetic model for peeling in the limit of a weakly non-equilibrium situation to establish a connection between thermally-activated barrier crossings and the equilibrium model. Here, we will develop a simple version that reduces to the expression for the low force limit (equation 6 in the main text) when thermal hopping rate is very high, i.e. as we approach thermal equilibrium.

Our system consists of the partially adsorbed ssDNA molecule subjected to displacement control, i.e. a fixed displacement, R, is applied by the AFM cantilever (one can obtain the same result under force control). We write the total free energy as a sum of three parts:

$$G = -n\,kT\ln(4\pi) - (N-n)\gamma b + \frac{3}{2}\frac{k_B T}{nb^2}R^2 \quad , \qquad \text{(S29)}$$

where n is the number of desorbed links, N is the total number of links, γ is the adhesion free energy per unit length, and b is the Kuhn length. The first term represents entropy gain on going from the surface to bulk, the second term is the free energy reduction due to adsorption, and the third term is free energy increase due to stretching (in a Gaussian chain approximation).

The second term, as written in Eq. S29, represents adsorption energy that increases monotonically with increasing number of bound bases and does not reflect the discrete (molecular) nature of the polymer chain. To reflect individual monomer units, we superimpose on top of the smooth variation in free energy a sinusoidal variation as individual bases adsorb or desorb (s measures the length of the contour that has desorbed from the substrate):

$$G_{total} = G + a\sin\left(\frac{2\pi s}{b}\right). \qquad \text{(S30)}$$

Figure S10 shows the free energy as a function of *s*. If the system is in equilibrium, then the average value of *s* is given by the global minimum in *G*. As we peel the molecule by increasing *R*, the minimum shifts to the right, and so does *s*.

The sinusoidal potential has a series of minima, which are traps for the base, and variation in *G* biases the traps so that, if its slope is positive, forward motion is slightly harder than backward motion. To first order, the energy barriers for forward and backward motion are, respectively:

$$\begin{aligned} &forward \quad 2a + \frac{dG}{ds}\frac{b}{2} \\ &back \qquad 2a - \frac{dG}{ds}\frac{b}{2} \end{aligned} \qquad \text{(S31)}$$

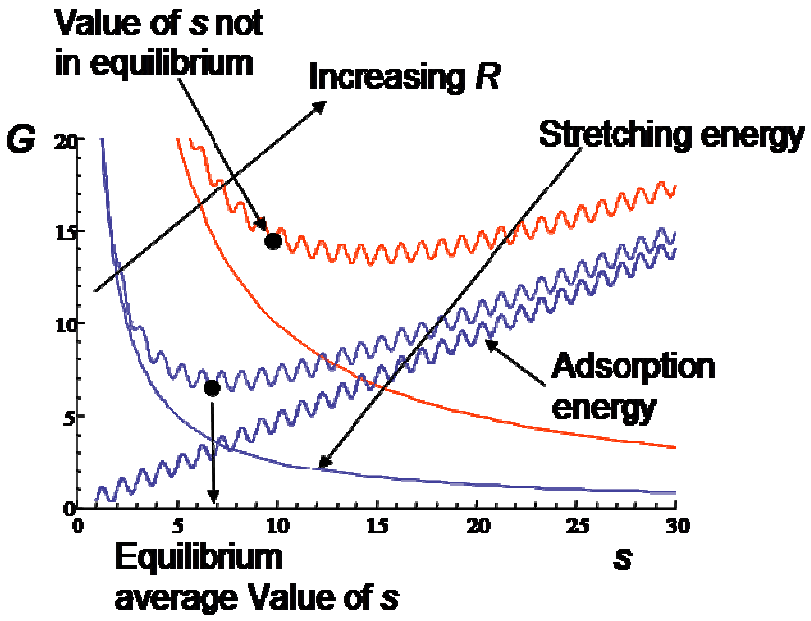

Figure S10. Free energy profile of partially desorbed and stretched oligomer. The adsorption free energy has an overall increase as the chain is desorbed but with undulations as individual bases are pulled off. The stretching energy has an overall decrease with increasing contour length of the desorbed molecule. As we peel off the molecule (increasing *R*), the minimum shifts to increasing *s*. If the system remains in equilibrium, the 'equilibrium' value of *s* shifts as the minimum of the free energy plot evolves.

Then, the rates of forward and backward hopping are given by (ν is an attempt frequency)

$$J_+ = \nu \exp\left(-\frac{2a + dG/ds(b/2)}{k_B T}\right)$$
$$J_- = \nu \exp\left(-\frac{2a - dG/ds(b/2)}{k_B T}\right) \quad \text{(S32)}$$

and the net flux is

$$\frac{dn}{dt} = J_+ - J_- = J_o \sinh\left(\frac{(-dG/ds)b}{2k_B T}\right) \approx J_o \frac{(-dG/ds)b}{2k_B T} \quad \text{(S33)}$$
$$J_o = \nu \exp(-2a/k_B T)$$

Here J_o is a reference unbiased hopping rate (in the absence of biases due to force loading).

Now, let us substitute the expression for *G*, Eq. S29, into Eq. S33 and use the fact that $s = nb$ to get

$$\frac{dn}{dt} = \left(\frac{kT \ln 4\pi}{b} + \frac{3}{2}\frac{kT}{n^2 b^3}R^2 - \gamma\right)\frac{J_o b}{2kT} \quad \text{(S34)}$$

which represents a kinetic model for peeling. At equilibrium, for fixed *R*, $dn/dt = 0$, and

$$n = \sqrt{\frac{3kT}{2b^3(\gamma - kT \ln 4\pi / b)}}\ R \quad \text{(S35)}$$

Force in a Gaussian spring is given by

$$f = \frac{3kT}{nb^2}R \quad \text{(S36)}$$

Eq. S35 and S36 combine to give us

$$\frac{\gamma b}{kT} = \ln(4\pi) + \frac{1}{6}\left(\frac{fb}{kt}\right)^2 \quad \text{(S37)}$$

which is the same as Eq. 6 in the manuscript (low force limit). In other words, as the kinetic model approaches equilibrium, it predicts a plateau force that is the same as that predicted by the equilibrium model.

In general, the nonlinear ordinary differential Eq. S34 can be solved with some initial conditions and some prescribed time evolution of *R(t)* to calculate how the molecule peels off. Let us look at a steady state case of linear tip velocity:

$$R = vt$$
$$\frac{dn}{dt} = \frac{v}{b} \tag{S38}$$

where v is the velocity of AFM tip retraction. These conditions convert Eq. S34 into an algebraic equation:

$$\frac{v}{b} = \frac{J_o b}{2kT}\left(\frac{3}{2}\frac{kT}{n^2 b^3}v^2 t^2 - \gamma + bkT\ln 4\pi\right) \tag{S39}$$

which can be solved for n, yielding

$$n = R\sqrt{\frac{3J_o}{4b^2\left[\frac{v}{b} + \frac{(\gamma - bkT\ln 4\pi)b}{2kT}\right]}} \tag{S40}$$

Combining this result with Eq. S36, we find that the peeling force is

$$f = \frac{2\sqrt{3}kT}{b}\sqrt{\frac{v/b + (\gamma - bkT\ln 4\pi)J_o b/2kT}{J_o}} \tag{S41}$$

Two features of this result are noteworthy: i) the force is constant, i.e., independent of R even in the case where we are not in equilibrium (force plateau develops), and ii) in the limit of large J_o, when we should approach equilibrium, we get the same velocity-independent force as predicted by the equilibrium model. In the limit of high velocities, or low J_o, that is when the system is straying from equilibrium, the peel force increases as the square-root of velocity.

REFERENCES AND NOTES:

1. Fujihira, M.; Okabe, Y.; Tani, Y.; Furugori, M.; Akiba, U. *Ultramicroscopy* **2000,** 82, (1-4), 181-191.
2. Herne, T. M.; Tarlov, M. J. *Journal of the American Chemical Society* **1997,** 119, (38), 8916-8920.
3. Lee, C. Y.; Gong, P.; Harbers, G. M.; Grainger, D. W.; Castner, D. G.; Gamble, L. J. *Analytical Chemistry* **2006,** 78, (10), 3316-3325.
4. Mourougou-Candoni, N.; Naud, C.; Thibaudau, F. *Langmuir* **2003,** 19, (3), 682-686.
5. Castner, D. G.; Hinds, K.; Grainger, D. W. *Langmuir* **1996,** 12, (21), 5083-5086.
6. Kudera, M.; Eschbaumer, C.; Gaub, H. E.; Schubert, U. S. *Advanced Functional Materials* **2003,** 13, (8), 615-620.
7. Zhang, Y. H.; Liu, C. J.; Shi, W. Q.; Wang, Z. Q.; Dai, L. M.; Zhang, X. *Langmuir* **2007,** 23, (15), 7911-7915.
8. Hutter, J. L.; Bechhoefer, J. *Review of Scientific Instruments* **1993,** 64, (7), 1868-1873.

9. Russel, W. B.; Saville, D. A.; Schowalter, W. R., Colloidal Dispersions. In Cambridge University Press: 1989.
10. Israelachvili, J., *Intermolecular and surface forces*. Academic Press: San Diego, 1992.
11. Khripin, C.; Jagota, A.; Hui, C. Y. *Journal of Chemical Physics* **2005,** 123, (13), 134705.
12. Reddy, S. Y.; Leclerc, F.; Karplus, M. *Biophysical Journal* **2003,** 84, (3), 1421-1449.
13. Foloppe, N.; MacKerell, A. D. *Journal of Computational Chemistry* **2000,** 21, (2), 86-104.
14. Manohar, S.; Tang, T.; Jagota, A. *Journal of Physical Chemistry C* **2007,** 111, (48), 17835-17845.
15. Leach, A. R., Molecular Modeling: Principles and Applications. In Prentice Hall: New York, 1996; pp 561-568.
16. Dill & Bromberg, *Molecular Driving Forces*, Garland Science (2003).